University Library



A gateway to Melbourne's research publications

Minerva Access is the Institutional Repository of The University of Melbourne

Author/s:
Beach, MA;Davey, TW;Subramanian, P;Such, GK

Title:
A self-healing waterborne acrylic latex coating based on intrinsic hydrogen bonding

Date:
2024-03

Citation:
Beach, M. A., Davey, T. W., Subramanian, P. & Such, G. K. (2024). A self-healing waterborne acrylic latex coating based on intrinsic hydrogen bonding. Progress in Organic Coatings, 188, https://doi.org/10.1016/j.porgcoat.2023.108189.

Persistent Link:
https://hdl.handle.net/11343/340261

License:
CC BY

Progress in Organic Coatings 188 (2024) 108189

Contents lists available at ScienceDirect

Progress in Organic Coatings

journal homepage: www.elsevier.com/locate/porgcoat

A self-healing waterborne acrylic latex coating based on intrinsic hydrogen bonding

Maximilian A. Beach [a], Tim W. Davey [b], Priya Subramanian [b], Georgina K. Such [a,*]

[a] Department of Chemistry, The University of Melbourne, Parkville, Victoria 3010, Australia
[b] DuluxGroup Australia, Clayton, Victoria 3168, Australia

ARTICLE INFO

Keywords:
Self-healing
Organic coatings
Acrylic latex
Extrinsic
Intrinsic

ABSTRACT

Acrylic coatings suffer damage in the form of cracking, which degrades both their protective and aesthetic performance over time. Self-healing technology offers the ability to solve this problem by allowing cracks to spontaneously heal without external diagnosis or intervention, offsetting the enormous costs associated with coating damage and repair. However, there is currently no efficient self-healing acrylic coating design, and research in the area remains noticeably sparse. In this research we sought to imbue a mechanically tough methyl methacrylate (MMA)/butyl acrylate (BA)/acrylic acid (AA) acrylic coating with self-healing functionality by incorporating self-healing monomers within the formulation. We synthesized a library of four acrylic monomers containing both a long amphiphilic spacer of variable length, and the 2-ureido-4[1H]-pyrimidinone (UPy) unit, which forms strong self-complementary quadruple hydrogen bonds. These UPy-monomers were able to participate in the emulsion polymerization of MMA, BA and AA, forming intrinsic hydrogen bonding networks within the subsequent acrylic coatings. These UPy functionalized coatings displayed optical self-healing and strain recovery over 24 h both at room temperature (~28 %), and at elevated temperatures up to 50 °C (~80 %). The coatings also displayed repeatable self-healing after four healing cycles, relative to an MMA/BA/AA coating.

1. Introduction

Coatings play a vital role in society by protecting surfaces from damage while at the same time imparting a variety of functional and aesthetic qualities. The coatings market is vast, and primarily composed of epoxy and polyurethane based coatings as well as acrylic coatings which are based on a suspension of polymer particles in water (latex). These coatings are commonly referred to as paints [1]. All coatings fall victim to a variety of stresses over time, leading first to the formation of cracks, and subsequently the total failure of the coating [2]. Replacement of the failed coating is expensive, time consuming and energy intensive. Thus, with the rapid development of self-healing technology since 2001, there exists a strong incentive to develop self-healing coatings [3].

Self-healing coatings can be defined as coatings which are able to heal damage spontaneously and without intervention. Based on their healing mechanisms, self-healing coatings can be divided into two categories: extrinsic and intrinsic [4]. Extrinsic self-healing is based on a healing agent which is added as a distinct component separate from the coating itself. Normally this involves encapsulating the healing agent within microcapsules, or occasionally microfibers, dispersed throughout the coating [5]. Following cracking, the microcapsules are ruptured, allowing the healing material to flow into the crack and initiate self-healing [6]. This healing normally occurs via auto-polymerization in the presence of a catalyst. Extrinsic self-healing strategies have been shown to yield high self-healing efficiencies for coatings, mainly epoxy resins [7–10]. However, the applicability of extrinsic self-healing strategies is limited by cost, the presence of microcapsules, which can alter the mechanical and optical properties of the coating, and the fact that a given damage area can heal only once [11,12]. Intrinsic self-healing coatings, on the other hand, have their healing functionality as part of the material itself. In the case of polymeric coatings, this normally involves the presence of reversible covalent or supramolecular bonds, which can reform following a damage event via attractive forces [13]. Dynamic covalent bonds, such as the disulfide bond, and reversible covalent reactions such as the Diels–Alder reaction/retro reaction, have been used to synthesize healable epoxy resins and polyurethane coatings. However, these coatings require high temperatures (>100 °C) to initiate the self-healing process, limiting their real-world applicability [14–16]. Supramolecular interactions such as hydrogen bonding, π-π

* Corresponding author.
E-mail address: gsuch@unimelb.edu.au (G.K. Such).

https://doi.org/10.1016/j.porgcoat.2023.108189
Received 25 October 2023; Received in revised form 15 December 2023; Accepted 21 December 2023
Available online 10 January 2024
0300-9440/© 2024 The Authors. Published by Elsevier B.V. This is an open access article under the CC BY license (http://creativecommons.org/licenses/by/4.0/).

stacking, electrostatic interactions and metal-ligand coordination bonds have shown the ability to impart polymer matrixes with robust self-healing at ambient temperatures [17–19]. Yet supramolecular self-healing is normally limited to softer low-modulus materials such as hydrogels, given that this healing relies on the rearrangement of polymer chains. Thus, imbuing stronger stiffer coatings with intrinsic self-healing functionality to allow for ambient self-healing represents a fundamental dilemma in materials science [20].

Nevertheless, recent efforts have been made to resolve this seeming contradiction. Stiffer polymeric materials have shown self-healing capability by combining a hard block, which utilizes higher Tg polymers to provide mechanical strength, with a soft block that provides the flexibility necessary for intrinsic self-healing. For example, copolymers containing a hard block such as poly(methyl methacrylate) (PMMA) or polystyrene (PS) and a soft polyacrylate amide block have shown the ability to heal materials with tensile strengths between 30 and 80 MPa [21,22]. A polymeric film containing a hard PS block and a soft poly (butyl acrylate) (PBA) block functionalized with the hydrogen bonding unit 2-ureido-4[1H]-pyrimidinone (UPy) was able to self-heal at only 45 °C and recover 90 % of its original tensile strength (up to 40 MPa) [23]. First developed by Meijer, the UPy unit forms strong, self-complementary quadruple hydrogen bonds, and thus has been extensively employed for the development of intrinsic self-healing materials [24]. UPy-based intrinsic self-healing materials such as hydrogels have shown strong self-healing at ambient conditions. The UPy unit has also been introduced to stronger materials such as epoxy and polyurethane coatings, allowing self-healing under more moderate conditions [25,26].

Despite the myriad of self-healing strategies presently available, research regarding self-healing acrylic coatings, as opposed to epoxy resins, polyurethane coatings and specialized anti-corrosive coatings, is lacking. In 2018, Cui et al. designed a self-healing acrylic coating based on the electrostatic attraction between poly(ethylene imine) (PEI) and poly(acrylic acid) (PAA) [27]. This design was able to self-heal when immersed in salt water, which helped plasticize the coating. UPy-based hydrogen bonding was used by Qiu et al. to imbue an MMA/BA acrylic coating with self-healing capability [28]. Their design incorporated a UPy functionalized monomer, dissolved in chloroform, to form coatings that displayed self-healing at 100 °C. Despite these limited studies, acrylic coatings which can heal under moderate conditions relevant to real-world applications remains a serious challenge.

Herein, we present a waterborne MMA/BA/AA acrylic coating which exhibits self-healing capability under ambient conditions, and across a range of temperatures up to 60 °C (Fig. 1). This was achieved through the incorporation of an acrylic UPy-functionalized monomer with a long polyethylene glycol (PEG) spacer. Such a PEG spacer allows for greater UPy chain mobility and is inspired by previous work into hard-soft block copolymer designs. The incorporation of a PEG spacer also allows the highly insoluble UPy monomer to transport through the water phase of an emulsion, and polymerize to form part of the waterborne latex without the need for large amounts of organic solvent [29]. Specifically, we synthesized a library of four different UPy monomers with various PEG spacer lengths, termed UPy-1, UPy-2, UPy-3 and UPy-4. UPy-1 represented the most hydrophobic design, with no PEG spacer, while the other three UPy monomers had PEG chains with molecular weight (MW) of 360, 500 and 2000 Da respectively. We compared these four UPy monomers to investigate how solubility and spacer length ultimately impacted self-healing capability. It was found that both UPy-2 and UPy-3 exhibited self-healing capability whose efficiency increased as the temperature increased from 25 °C to 60 °C. Of these two designs, UPy-2, with a longer PEG spacer, was noticeably superior. Furthermore, the UPy-2 coating was able to self-heal a crack over three damage/healing cycles, which is a key advantage of intrinsic, as opposed to extrinsic, self-healing designs. This work demonstrates a novel example of ambient self-healing both for acrylic coatings, an under-researched area in self-healing literature, and for stiffer, more rigid coatings, which remains a challenge for intrinsic self-healing strategies. Our research also provides an important understanding of the mechanisms necessary for efficient intrinsic self-healing. Ultimately, such research represents an important step toward the design of self-healing commercial paints.

2. Experimental

2.1. Materials

2-Amino-4-hydroxy-6-methylpyrimidine, ethanolamine, methacroyloyl chloride, hydroquinone, triethylamine (TEA), 1,1′-carbonyldiimidazole (CDI), poly(ethylene glycol) methacrylate (PEGMA) (molecular weight (MW) = 500 and 360), polyethylene glycol (PEG) (MW = 2000), hexamethylene diisocyanate, dibutyl tin dilaurate

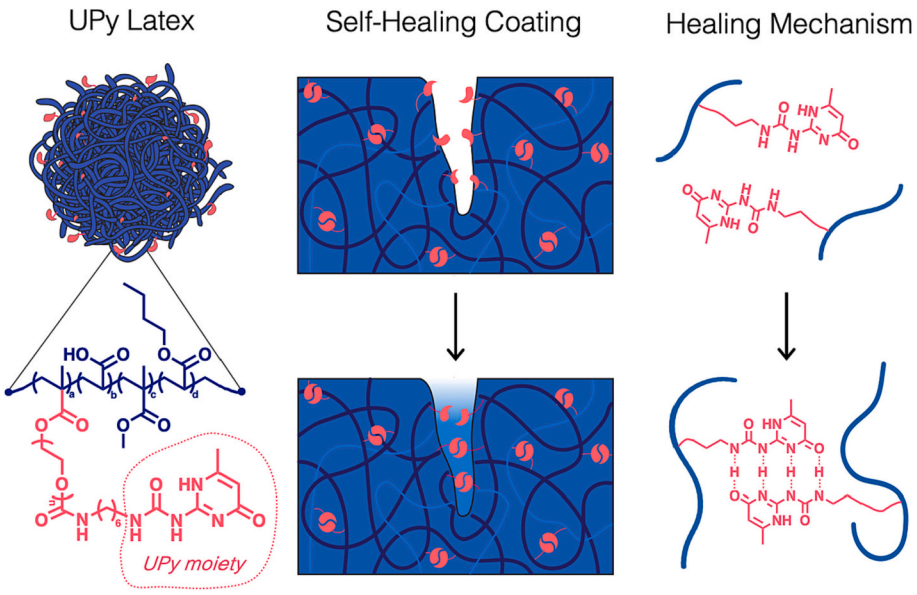


Fig. 1. The concept of a self-healing acrylic coating. First, the hydrogen bonding unit UPy is incorporated into acrylic latex particles via the polymerization of a UPy-functionalized acrylic monomer. Then, as water evaporates, these latex particles coalesce to form an acrylic coating with a UPy-based hydrogen bonding network. Finally, following damage to the coating, intrinsic self-healing is generated through the attractive self-complementary hydrogen bonding of the UPy moieties.

catalyst, as well as methyl methacrylate (MMA), butyl acrylate (BA), acrylic acid (AA), and sodium dodecyl sulfate (SDS) were all purchased from Sigma Aldrich and used as received. Ammonium persulfate, as well as the solvents dimethyl sulfoxide (DMSO), chloroform ($CHCl_3$), ethyl acetate, diethyl ether, acetone, pentane, hexane, methanol, dichloromethane (DCM) and dimethylformamide (DMF) were purchased from ChemSupply Australia. The deuterated solvents $CDCl_3$ and DMSO were purchased form Sigma Aldrich. The 3.5 kDa MWCO dialysis 'snakeskin' bag (Thermo-Fischer Scientific) was used according to instructions.

2.2. Characterization

^{1}H NMR spectroscopy was performed on a 400 MHz Varian 400 MR spectrometer using deuterated chloroform ($CDCl_3$) as the solvent. ^{1}H NMR analysis was performed on MestreNova software. GPC analysis was performed on a Shimadzu system equipped with a Waters Styragel column (10 μm pore size). THF was used as the eluent with a flow rate of 1 mL/min. The molecular weight and polydispersity of the samples were calculated relative to poly(methyl methacrylate) (PMMA) standards. Samples were prepared at 2 mg/mL and filtered (0.45 μm) prior to measurement. IR spectroscopy was performed on a Perkin Elmer Spectrum 2 ATR-FTIR spectrometer, and UV Vis spectroscopy was performed on Cary 60 UV–Vis (Agilent technologies). Dynamic light scattering analysis of particle size was performed on a Horiba Nanopartica SZ-100 (Horiba Scientific, Japan), operating at 37 °C and a fixed scattering angle of 90°. Optical microscopy images were taken on an optical microscope and TEM images were recorded on a FEI Talos L120C cryoTEM. Surface measurements were performed on a Bruker ContourGT Optical Profilometer. Tensile tests were carried out on an Instron 5944, 2 kN microtester. Differential scanning calorimetry was performed on a Perkin Elmer 8500 Double Furnace HyperDSC from −50 to 70 °C at 10 °C/min.

2.3. Synthesis of 2-aminoethyl methacrylate (**2**)

Ethanolamine (1.21 g, 12.5 mmol) and hydroquinone (0.01 g, 0.1 mmol) were mixed in a round bottom flask equipped with a condenser. The mixture was heated to 95 °C under nitrogen. Methacryloyl chloride (1) (2 mL, 18.4 mmol) was slowly added to the mixture over the course of an hour with vigorous stirring. The mixture was further stirred for half an hour and then cooled to 60 °C. The product in the form of a white powder (yield: 94 %) was precipitated in ethyl acetate. ^{1}H NMR (400 MHz, $CDCl_3$): δ (ppm) 6.1 and 5.6 (C–CH_2), 4.3 (CH_2–CH_2–O), 3.3 (CH_2–CH_2–O), and 1.8 (OC–CCH_2–CH_3) (Fig. S1).

2.4. Synthesis of N-(6-methyl-oxo-1,4-dihydropyrimidin-2-yl)-1H-imidazole-1-carboxamide (**4**)

2-Amino-4-hydroxy-6-methylpyrimidine (3) (1.5 g, 12 mmol) was dissolved in 15 mL DMSO. 1,1′-Carbonyldiimidazole (2.52 g, 15 mmol) was added and the mixture was stirred for 24 h at 80 °C under nitrogen. The mixture was then cooled to room temperature and acetone was added to precipitate the product. The precipitant was collected by filtration and washed with acetone. The white powder product, henceforth known as UPy-imidazole, was dried under vacuum (Yield: 90 %). ^{1}H NMR (400 MHz, DMSO): δ (ppm) 7.6 (N–C*H*–N Imidazole), 7.1 (N–C*H*–CH–N Imidazole), 6.9 (N–CH–C*H*–N Imidazole), 5.4 (OC–C*H*–CCH_3), and 1.9 (OC–CH–CCH_3) (Fig. S2).

2.5. Synthesis of 2(6-isocyanatohexylaminocarbonylamino)-6-methyl-4 [1H] pyrimidinone (**5**)

2-Amino-4-hydroxy-6-methylpyrimidine (3) (1.0 g, 8.0 mmol) was added in hexamethylene diisocyanate (8.0 g, 48 mmol). The mixture was then heated to 100 °C and stirred for 20 h under nitrogen. After this time, 20 mL of pentane was added to precipitate the product. The product was dried under vacuum to yield a white powder (yield: 95 %). ^{1}H NMR (400 MHz, DMSO): δ (ppm) 5.8 (OC–C*H*–CCH_3), 3.2 (Hexyl chain), 2.2 (CH_3–C–NH), 1.4–1.6 (Hexyl chain), 10.6, 12.0 and 13.1 (hydrogen bonding peaks of UPy) (Fig. S4). FTIR: v 2900 (CONH), 2270 (NCO), 1700 (aryl C═O) 1650 (NCON) and 1100 (C—O) (Fig. S5).

2.6. Synthesis of the UPy monomer, UPy-1

UPy-imidazole (**4**) (0.5 mmol, 110 mg) and 2-aminoethyl methacrylate (**2**) (0.75 mmol, 120 mg) were dissolved in 10 mL of dry DMF. 120 μL of TEA base was added and the reaction was stirred under nitrogen at room temperature overnight. The product was precipitated with water, and washed with water and acetone, before being vacuum dried to yield a white powder (yield: 90 %). ^{1}H NMR (400 MHz, $CDCl_3$): δ (ppm) 6.2 and 5.8 (OC–CCH_2–CH_3), 5.6 (OC–C*H*–CCH_3), 4.3 (CH_2–CH_2–O), 3.6 (CH_2–CH_2–O), 2.2 (OC–CH–CCH_3), 1.8 (OC–CCH_2–CH_3), 10.5, 12.0 and 13.0 (hydrogen bonding peaks of UPy) (Fig. S3).

2.7. Synthesis of the UPy monomer, UPy-2

2(6-Isocyanatohexylaminocarbonylamino)-6-methyl-4[1H] pyrimidinone (**5**) was added to a solution of poly(ethylene glycol) methyl methacrylate (PEGMA) (MW = 500 Da) in dry chloroform at an even mol ratio. The mixture was heated to 60 °C under a nitrogen atmosphere, and a few drops of the catalyst, dibutyl tin dilaurate, were added. The reaction was then left to stir until all of the isocyanate precursor had converted. This was monitored via the IR peak at 2200 cm^{-1}. The product was then dried under vacuum (yield: ~98 %). ^{1}H NMR (400 MHz, $CDCl_3$): ∂ (ppm) 6.1 and 5.6 (CH_3–CCH_2–CO), 5.8 (OC–C*H*–CCH_3), 4.0–4.4 and 3.6–3.8 (PEG chain), 3.1–3.4 (Hexyl chain), 2.2 (CH_3–C–NH), 1.8 (CH_3–CCH_2), 1.4–1.6 (Hexyl chain), 10.5, 12.0 and 13 (UPy hydrogen bonds) (Fig. S6). FTIR: v 2900 (CONH), 1700 (aryl C═O), 1650 (NCON) 1100 (C—O) (Fig. S7). The UPy monomers, UPy-3 (Fig. S8–9) and UPy-4 (Fig. S11–12), were synthesized as per the synthesis of UPy-2, however using PEGMA with MW = 360 and ~2000 Da respectively.

2.8. Synthesis of PEGMA (MW ~ 2000 Da)

Poly(ethylene glycol) (MW ~ 2000 Da) (6) (3.5 g, 1.75 mmol) was dissolved in 60 mL of dry dichloromethane and stirred under nitrogen. As the mixture was cooled to 0 °C in an ice bath, 245 mg of triethylamine (1.4 eq.) was added dropwise into the solution. Once the mixture had reached 0 °C, 218 mg of methacryloyl chloride (1) (1.2 eq.) was slowly added dropwise over a period of 1 h. Following this, the reaction was left to stir at room temperature overnight. The resulting mixture was washed with 0.1 M HCl, followed by saturated $NaHCO_3$ solution and finally by brine. The crude product was then recrystallized in cold diethyl ether (yield: 84 %). ^{1}H NMR (400 MHz, $CDCl_3$): ∂ (ppm) 6.1 and 5.6 (CH_3–CCH_2–CO), 4.0–4.4 and 3.6–3.8 (PEG chain), and 1.8 (CH_3–CCH_2) (Fig. S10).

2.9. Emulsion polymerization

Emulsion nanoparticles were synthesized with the following procedure:

Reactants	Solids (wt%)
Butyl acrylate	47
Methyl methacrylate	47
Acrylic acid	2
UPy monomer	2.5
Sodium dodecyl sulfate (surfactant)	1.2
Ammonium persulfate (initiator)	0.3

The emulsion was performed in deionized water with a solid content of 20 wt%. Initially, a solution of de-ionized water and dissolved surfactant (sodium dodecyl sulfate) was deoxygenated under a nitrogen atmosphere and heated until the internal temperature rose to 80 °C. Following this, two separate feeds were prepared. The first was the monomer feed containing butyl acrylate, methyl methacrylate and acrylic acid (feed 1, S29). The UPy monomer (2.5 wt%) was added to this feed, and the solution was sonicated for 30 s. The second feed was the initiator (ammonium persulfate) dissolved in deionized water which was made up to the same volume as the monomer feed. Following the sonication of feed 1, both feeds were simultaneously fed into the reactor over a 3 h period. After feeding, the reaction was left to run for a further hour for a total reaction time of 4 h. The resulting latex was purified via dialysis for a week (MWCO 3.5 kDa), displacing water twice a day. The latexes were characterized by ^{1}H NMR and UV–Vis spectroscopy to verify the presence of UPy monomer. DLS and TEM were employed to understand the shape and size of the latex particles.

2.10. Pencil hardness test

The surface hardness of the coatings was determined via the pencil hardness test. The coatings were cleaned to remove and dust or other impurities on the surface. A series of pencils ranging in hardness from 6B to 2H were conditioned by grinding on a piece of abrasive paper. The pencils were checked to make sure the edges of the graphite were smooth and level, not nipped or chipped. The pencils were then placed at a 45° angle to the coating and pushed forward with firm pressure. The hardness was defined as the hardest pencil which fails to cut the film, and the experiment was performed three times with a fresh pencil edge.

2.11. Water resistance test

The water resistance of the coatings was determined gravimetrically. The coatings were immersed for 24 h under four different conditions: Deionized (neutral) water, saturated salt water, acidic (pH 5) water and 60 °C water. The weight gain after immersion was measured and reported as a fraction of the total weight.

2.12. Film formation and self-healing tests

To form the coatings, the latex was added to a silicone mold (30 mm × 30 mm × 1 mm) and left to dry at room temperature for 1 week and then at 50 °C for 2 days. As the water evaporated, the latex particles coalesced, forming the acrylic coating. Following this, the coating was cut into a rectangular shape (30 mm × 12 mm × 600 μm). A 5 mm long horizontal cut was introduced to the coating via a razor blade, and penetrated the coating completely, with a depth of 600 μm. This cut was allowed to heal at room temperature over 24 h with no intervention. Optical self-healing tests were performed via an optical microscope and a surface profilometer. The self-healing behavior of the coating was photographed, and a 3D rendering of the surface topology was generated, yielding the depth and width of the crack at its widest point.

Tensile tests were carried out under the following conditions: a strain rate of 3 mm/min, a gauge length (fixture separation) of 17 mm and a temperature of 25 °C. An average result was calculated from three independent experiments. To evaluate the strain recovery of the coatings (a measure of self-healing efficiency), a 5 mm long horizon cut was introduced to the coating via a razor blade. The coatings were then gently pressed together for 5 s and left to heal for 24 h over a given healing temperature (25, 40, 50 or 60 °C). The healed samples were then subject to tensile tests. The Young's modulus (E) and the strain at which the healed crack reopened (ε, strain-at-break, failure strain) was noted and compared to the strain at which an undamaged coating began to break apart. Given the malleability of the coatings, there was no sudden fracturing of the undamaged coating, rather, the failure strain was noted when the crack opened and the coating began to 'unzip'. This is contrasted with what is often defined as the strain-at-break for brittle materials, where the material breaks suddenly into two parts.

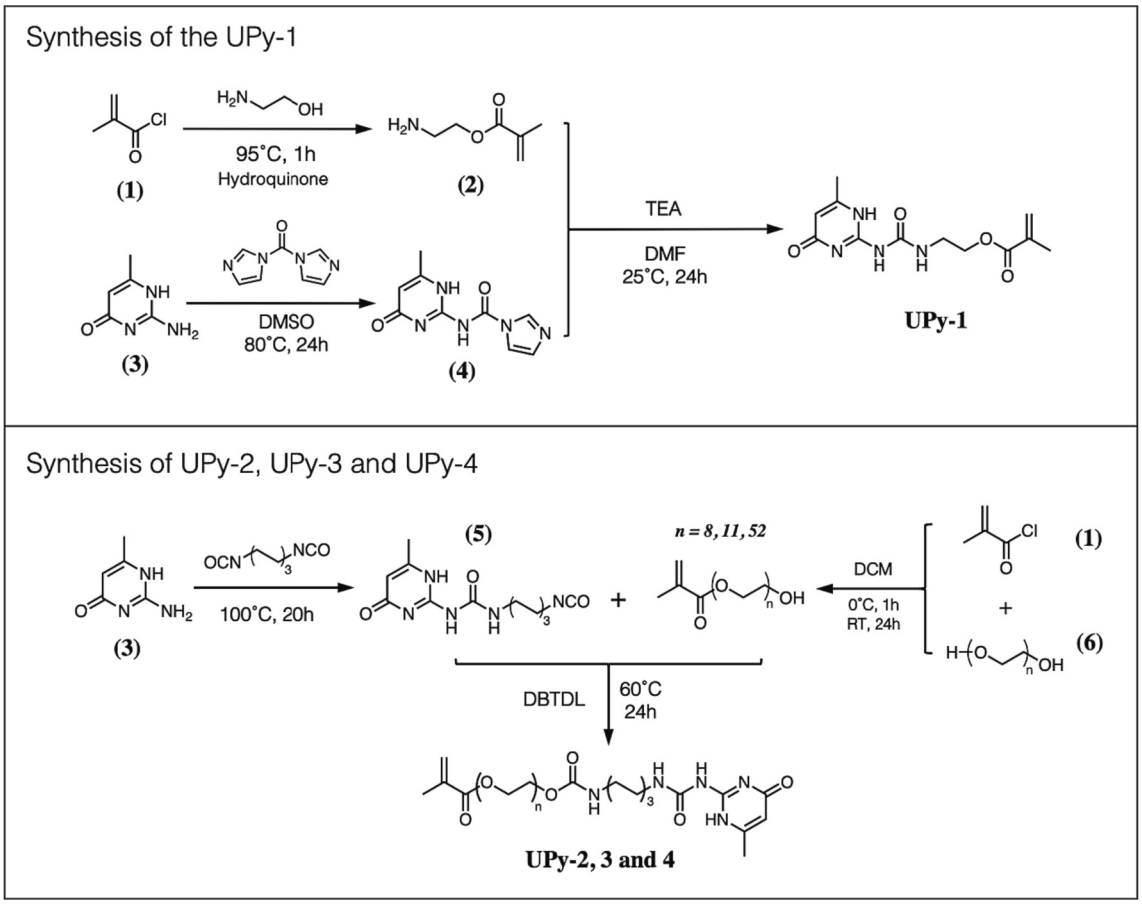
3. Results

A library of four UPy-functionalized acrylic monomers were synthesized with varying PEG spacer lengths (Scheme 1, Fig. 2). The monomer UPy-1 (Fig. S3) was synthesized through the precursor UPy-imidazole (Fig. S2), which then underwent a highly efficient nucleophilic addition reaction with aminoethyl methacrylate (Fig. S1). UPy-1 represents the most hydrophobic possible UPy functionalized monomer, and lacks any PEG spacer separating its strong hydrogen bonding unit from the polymer backbone. The other three UPy monomers were synthesized via a two-step isocyanate-hydroxyl reaction, and contained both a long hydrophilic PEG spacer, and a hydrophobic hexyl chain end capped with the UPy unit, yielding amphiphilic character (Figs. S4–12). Hydrophobicity is necessary for the monomer to polymerize and form part of the latex, while the partial hydrophilicity of the PEG chain allows for monomer transport through the aqueous phase of the emulsion [29]. Furthermore, the long PEG spacer distances the UPy self-healing unit from the backbone of the hydrophobic polymer, potentially enhancing self-healing capability by maximizing the degrees of freedom of the UPy units. The synthesis of these monomers was highly efficient, generating high yields (>90 %) and was able to be performed under moderate conditions, chiefly due to the strength of the imidazole leaving group, in the case of UPy-1, and the reactivity of the isocyanate moiety, in the case of UPy-2 to 4.

All four of the UPy monomers were tacky solids, and highly insoluble in both water and organic solvents, with the exception of chloroform and DMF. This fact makes their incorporation into a solvent-free waterborne emulsion polymerization problematic. To test their stability, the four monomers were added to a BA/MMA/AA feed at a concentration of up to 5 wt%, and the solution was then sheared for 30 s of sonication to accelerate the dissolution of the UPy-monomers. Fig. 2 shows that only UPy-2 and UPy-3 could be stably incorporated into a BA/MMA/AA feed, each at a maximum concentration of 2.5 wt%. The fact that both UPy-1, the most hydrophobic design, and UPy-4, the most hydrophilic design, each had extremely poor solubility, implies the existence of an amphiphilic 'goldilocks zone', where both the hydrophobicity and hydrophilicity of UPy-2 and UPy-3 are sufficiently balanced to yield stability up to 2.5 wt%. Therefore, due to the insolubility of UPy-1 and UPy-4, only UPy-2 and UPy-3 were incorporated into a waterborne MMA/BA/AA latex.

UPy functionalized, waterborne MMA/BA/AA latexes were prepared through solvent-free emulsion polymerization. A monomer feed containing 2.5 wt% of either UPy-2 or UPy-3, and an initiator feed were added to an 80 °C reactor over 3 h. The polymerization continued for another hour, yielding a gravimetric monomer conversion of ~91–92 %. The resultant latexes were then dialysed to remove unreacted monomer. DLS and TEM showed spherical latex particles with average sizes of around 100 nm, with DLS yielding average latex particle diameters of 80 nm, 91 nm and 110 nm for the control, UPy-2 and UPy-3 latexes respectively (Fig. 3a–d). It is interesting to note that the dispersity of the latex particles increases slightly with the incorporation of the UPy functionalized monomers. This may be due to the strong self-complementary nature of the UPy units, causing a fraction of the nanoparticles to aggregate with each other, yielding larger particles and thus a higher dispersity. Nevertheless, all three latex particle samples are highly monodisperse. Furthermore, these latexes were also found to be highly stable over the course of a year, with the dispersity remaining essentially unchanged in the case of the control and UPy-3 latexes, while increasing from 0.1 to 0.3 between 6 and 12 months, in the case of the UPy-2 latex (Fig. S25).

The successful incorporation of UPy into the latexes was verified by ^{1}H NMR of the latex, via monitoring the peaks from 3.3 to 3.1 ppm, which corresponds to the hexyl chain spacer on the UPy monomer



Scheme 1. The synthesis of UPy-1, as well as UPy-2, UPy-3 and UPy-4.

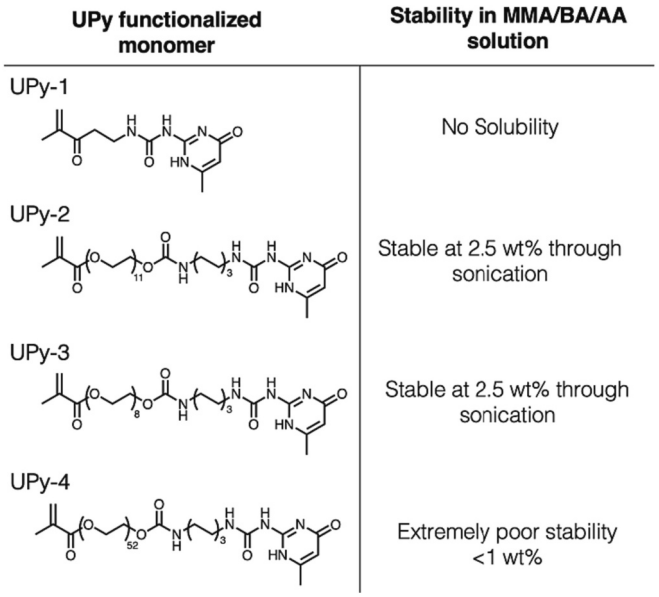


Fig. 2. The chemical structure of the four UPy functionalized monomers (UPy-1 to UPy-4), as well as their respective stabilities in the acrylic monomer feed (MMA/BA/AA).

(Fig. 3f, S13–15). These peaks do not appear in the control latex. The UPy unit absorbs light between 250 and 300 nm. Therefore, the amount of UPy in the latex can be further quantified through UV/Vis spectroscopy using a standard curve of known concentrations of each monomer (Fig. S16–17). 260 nm was selected to construct the absorbance calibration of UPy as it is distinct from the solvent cut off value (250 nm for $CHCl_3$). 250–300 nm is a relatively broad range of light absorption, and is due to the fact that UPy can form a variety of rotamers, as well as a tautomeric pyrimidin-4-ol conformation which absorbs ~290 nm [30]. At 260 nm, the absorbance is essentially independent of this UPy tautomeric conformation behavior [31]. At concentrations of 1 mg/mL, a shoulder is clearly visible between 250 and 300 nm for UPy-2 and UPy-3 latexes, and absent from the control latex, verifying the incorporation of the UPy functionalized monomers (Fig. 3e). Comparing these absorbance values with standard curves yields a UPy monomer conversion of 84 % for the UPy-2 latex, and 90 % for the UPy-3 latex. 90 % for UPy-3 is similar to the conversion of MMA and BA, which was calculated gravimetrically to be between 91 % and 92 %. However 84 % obtained for UPy-2 is a slight decrease in conversion relative to the other monomers. One explanation for this may be the slightly reduced monomer feed solubility of UPy-2 relative to UPy-3, given the longer hydrophilic PEG spacer, which could cause the loss of some UPy-2 during the emulsion. Nevertheless, both UPy-2 and UPy-3 are capable of incorporation into an acrylic latex via emulsion polymerization without the need for large amounts of organic solvent, a significant marker of a more robust self-healing design. UV/Vis was also used to analyze the transparency (opacity) of the three resultant coatings (Fig. S28). The coatings were transparent, with each having a transmittance of over 80 %. Importantly, the addition of UPy-2 and UPy-3 did not affect the transparency of the acrylic films.

Mechanical tests were carried out on the control coating without UPy monomer and the two coatings containing 2.5 wt% UPy-2 and UPy-3. The glass transition temperature (Tg) is the temperature at which an amorphous polymer matrix transitions from a glassy, brittle material to

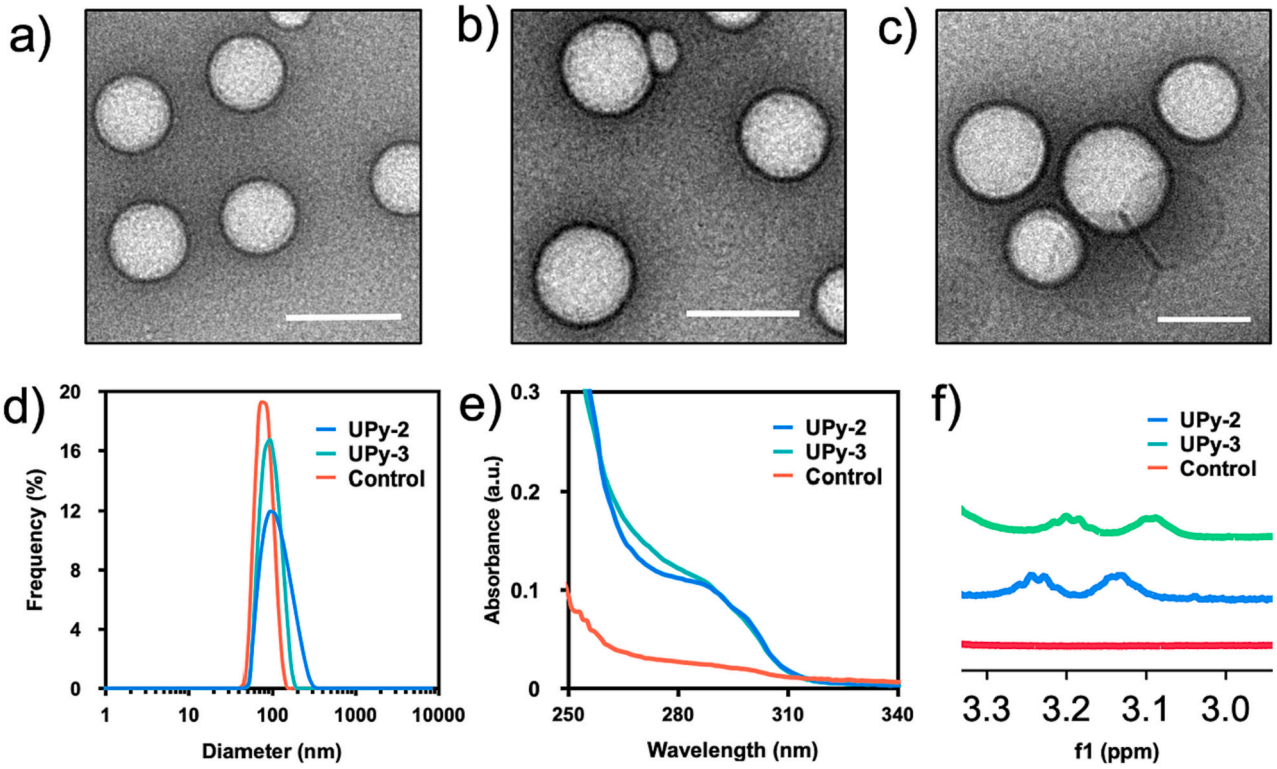


Fig. 3. Characterization of the UPy functionalized BA/MMA/AA latex. TEM images of the latex particles for the control latex (a), the UPy-2 latex (b), and the UPy-3 latex (c) showing sizes of approximately 80–100 nm. The scale bar in white represents 100 nm. d) DLS intensity size distribution of the control, UPy-2 and UPy-3 latex particles. e) UV Vis spectrum of the control, UPy-2 and UPy-3 latexes. The shoulder between 250 and 300 nm corresponds to the absorbance of the UPy unit. f) A zoomed in ^{1}H NMR spectrum of the control, UPy-2 and UPy-3 latexes, where the peaks between 3.1 and 3.2 ppm correspond to the hexyl chain of the UPy monomers.

a softer, plasticized substance. It is theorized that Tg plays an important role in intrinsic self-healing efficiency, given that polymer mobility and rearrangement is a far more pronounced above Tg [32]. Tg can be estimated according to Flory-Fox theory, and for a 1:1 BA/MMA latex with 2 % AA, the theoretical Tg is approximately 6 °C. The Tg of each coating was measured by DSC and, the results are shown in Fig. 4a and S18–20. All three coatings have a Tg higher than their theoretical Tg according to the Fox equation, while the range between the three coatings is very small (15–18 °C). The UPy monomer contains a long PEG spacer, who's low Tg (approximately −50 °C) would seemingly lower the Tg of the overall coating. However, other studies using UPy based monomers without flexible spacers, have reported slight increases in Tg, due to the hydrogen bonding interactions between the UPy units [33]. DSC measurements show that the UPy-2 and UPy-3 monomers have very limited effect on the Tg of the resultant coatings. Specifically, the control coating's Tg was measured at 18 °C, with the UPy-2 and UPy-3 coatings measured at 16 and 15 °C respectively.

The coatings were subjected to tensile testing to yield stress strain curves (Fig. 4b). Young's modulus, also known as the elastic modulus, is the ratio of stress to strain in the elastic deformation (linear region) of the curve, and measures how resistant a material is to deformation. It is the most common metric when defining and comparing the mechanical strength of different materials. Most intrinsic self-healing strategies rely on materials with a modulus from 0.1 MPa in the case of hydrogels to

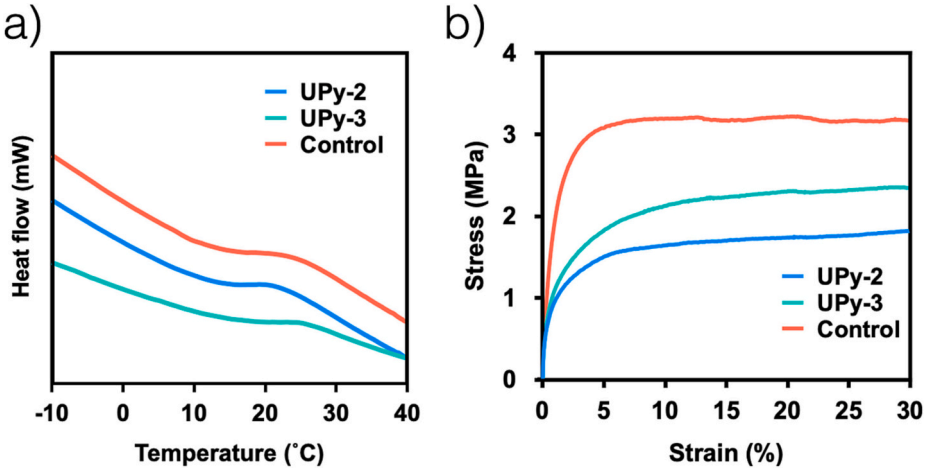


Fig. 4. Mechanical properties of the UPy functionalized MMA/BA/AA acrylic coatings. a) DSC heat flow curves of the control, UPy-2 and UPy-3 coatings yielded the Tg of the coatings. b) Stress-strain curves of the control, UPy-2 and UPy-3 coatings yielded the Young's modulus (stiffness) and the ultimate strength of the coatings.

~10 MPa in the case of stronger elastomers. Acrylic coatings, on the other hand, are generally stiffer materials with a Young's modulus >100 MPa. The control, UPy-2 and UPy-3 coatings each have a Young's modulus of 0.20 and 0.22 GPa respectively, which is well within the operational range of such coatings. The control coating, at 0.3 GPa is slightly stiffer than the UPy based coatings, while also having a higher ultimate stress (~3 MPa), further reinforcing the idea that the PEG chains on the UPy monomers slightly soften the resulting coatings. Though the tensile strengths of UPy-2 and UPy-3 coatings (~2.2 and ~1.6 MPa respectively) are reduced compared to the control, they are still well within the expected range for acrylic coatings of this kind [1,34]. Thus, our UPy functionalized acrylic coatings maintained favourable mechanical strength, with Young's moduli two orders of magnitude above hydrogels and elastomers, and a Tg similar to that of unaltered latex acrylic coatings.

As well as Tg and Young's modulus, the surface hardness of the coatings was examined via a pencil hardness test (Fig. S26). All three coatings displayed strong surface hardness, with the control and UPy-3 coatings displaying a hardness of H, and the UPy-2 coating displaying an average hardness of HB. Importantly, the addition of the UPy functionalized monomers did not significantly reduce the surface hardness of the resulting acrylic coating. The water resistance of each coating was measured gravimetrically under four separate conditions: de-ionized (neutral) water, saturated salt water, acidic (pH 5) water and hot water (60 °C) (Fig. S27). Poor water resistance in the form of water uptake is a drawback of waterborne emulsion systems. In neutral water, all three coatings gained ~10 % of their weight after 24 h, and this weight gain increased upon increasing temperature. Crucially, however, the addition of the UPy-2 and UPy-3 monomer did not alter the water resistance properties of the MMA/BA/AA control coating.

To determine whether the UPy functionalized acrylic coatings exhibited any self-healing performance, optical self-healing tests were conducted by introducing a crack through the coatings via a razor blade, and then allowing the coatings to spontaneously heal at room temperature. Fig. 5 displays images from the optical microscope immediately following the cutting of the films, and then after 24 h of healing time. The control coating clearly displays no self-healing after 24 h at room temperature, which is unsurprising, given the lack of UPy functionalization. However, as Fig. 5b–c show, both the UPy-2 and UPy-3 coatings displayed noticeable optical self-healing capability, with the UPy-2 coating showing significant self-healing particularly near the top of the crack, which is shown within the dotted line in Fig. 5b).

Fig. 5d shows the self-healing of UPy-2 coating after 24 h at 60 °C. Clearly the optical self-healing is significantly stronger than at room temperature, as the crack has fully closed, and the presence of damage is far more difficult to see. Interestingly, full optical healing of the crack, whereby there is almost no evidence of damage having ever occurred, remained absent, even when increasing the healing time over a week at 60 °C. Fig. 5 shows that the UPy-2 and UPy-3 functionalized acrylic coatings were able to spontaneously heal damage and display clear optical self-healing capability, which increased with elevated temperature. Optical profilometry was used to gain a more quantitative understanding of crack self-healing, showing that almost all crack depth was recovered in the case of the UPy-2 coating, and that the UPy-3 coating's crack had an average depth of ~100 μm (Fig. S30). Furthermore, the widths of the cracks drastically reduced following 24 h at room temperature, with UPy-3's width reducing by ~66 % and UPy-2's width decreasing by ~80 %, compared to the unhealed control.

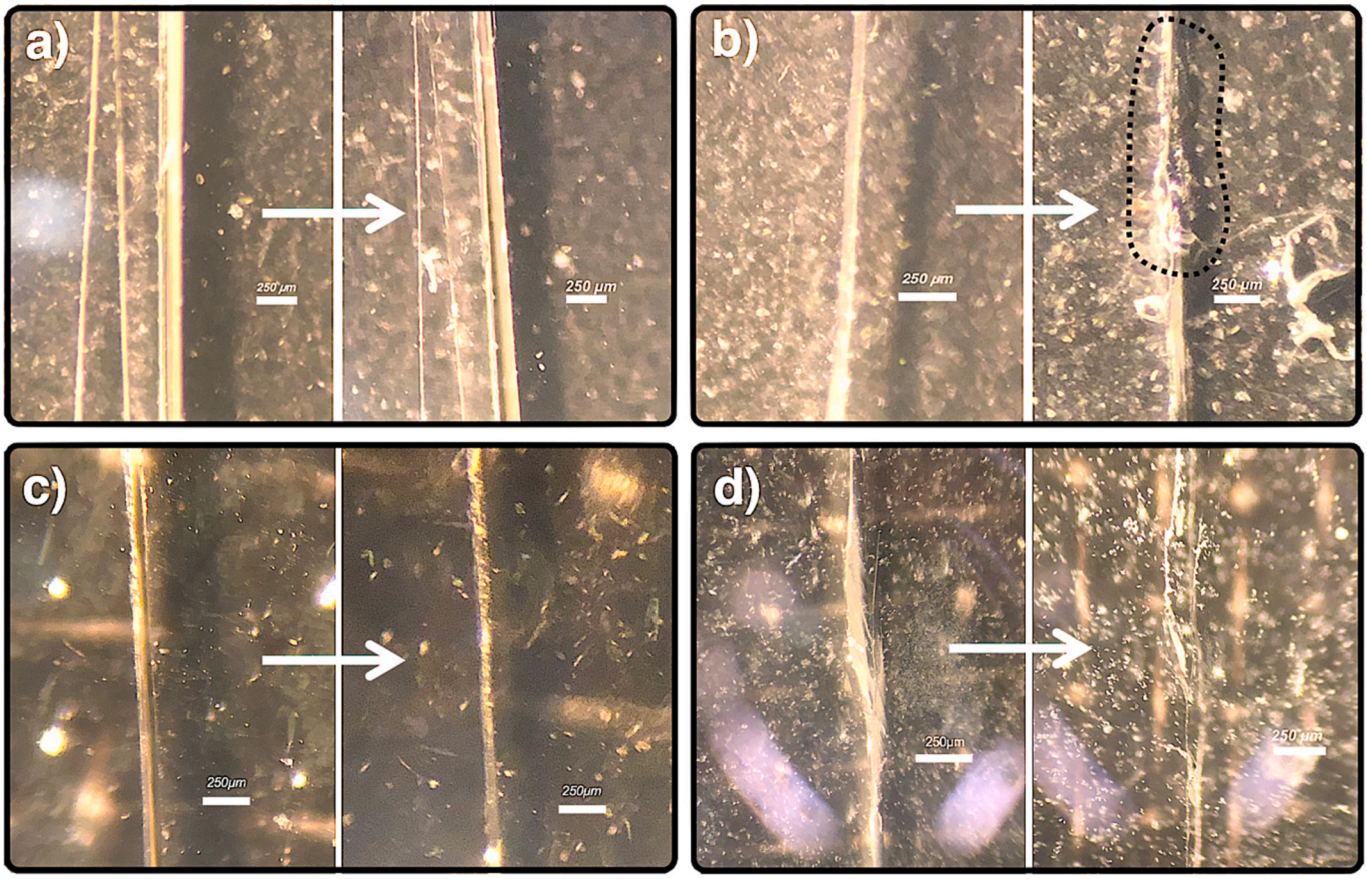


Fig. 5. Optical self-healing tests. The coatings were cut through with a razor blade, and images were taken with an optical microscope immediately (left image) and after 24 h at a given temperature (right image). a) Control coating at RT. b) UPy-2 coating at RT. c) UPy-3 coating at RT. d) UPy-2 coating at 60 °C. Scale bar represents 250 nm.

To understand more about the self-healing potential of these systems we measured the strain recovery of each coating to determine their self-healing efficiency. This method for calculating healing efficiency has been applied to various polymeric matrixes employing hydrogen bonding self-healing, including urea and barbiturate elastomers [35,36]. Self-healing efficiency was calculated via the ratio between the strain-at-break of the undamaged coating and the damaged coating after a given set of self-healing conditions. Some materials are brittle and fracture sharply and completely, however polymeric coatings including acrylic coatings deform and elongate before eventually fracturing in the form of a crack which gradually 'unzips'. We defined the strain-at-break for the virgin coating as the point at which fracture in the form of an open crack first appears, before the crack unzips and the coating rips in half. The strain-at-break for the healed coating was defined as the strain at which the healed crack initially opens. For healed samples, the crack does not open up all at once, rather it opens from the center first, and unzips outwards.

A cut was introduced to the control coating, along with UPy-2 and UPy-3 coatings via a razor blade and the samples were allowed to heal over 24 h for a variety of different temperatures (Fig. 6c, S21–22). At room temperature, both UPy coatings displayed self-healing activity in the form of strain recovery, with the UPy-2 coating having a higher strain recovery (~28 %) compared to the UPy-3 coatings (~12 %) (Fig. 6a–c). The control coating, containing no UPy functionality, had no self-healing capability at room temperature, as upon tensile stress, the crack opened immediately. Fig. 6c shows that self-healing efficiency increases with temperature, from ~60 % at 40 °C to ~80 % at 50 °C in the case of UPy-2, and from ~30 % at 40 °C to ~60 % at 50 °C in the case of the UPy-3 coating. At all three temperatures, there is a statistically significant difference between the self-healing efficiency of the UPy functionalized coatings and the control coating, indicating that the UPy moiety yields noticeable self-healing performance, due to the strong self-complementary hydrogen bonding.

The difference in healing performance between the UPy-2 and UPy-3 coatings suggests that the length of the spacer between the UPy unit and the polymer backbone impacts self-healing capacity. The superior self-healing efficiency of the UPy-2 coating is likely due to its longer poly (ethylene glycol) spacer, which increases polymer chain translational and rotational mobility, allowing the UPy units to rearrange and self-heal more efficiently. Furthermore, the elevated distance between the UPy unit and the polymer backbone likely reduces steric hindrance, which further enhances the ability of the UPy units to self-complement. Such enhanced polymer chain mobility is also the reason why self-healing performance increases with elevated temperature, as for polymeric materials, high temperatures maximize polymer chain mobility. Previous work on polymers with UPy functionalized backbones has also shown an increase in the association/dissociation dynamics of UPy at temperatures above 40 °C [37]. Interestingly, above 60 °C, the strain

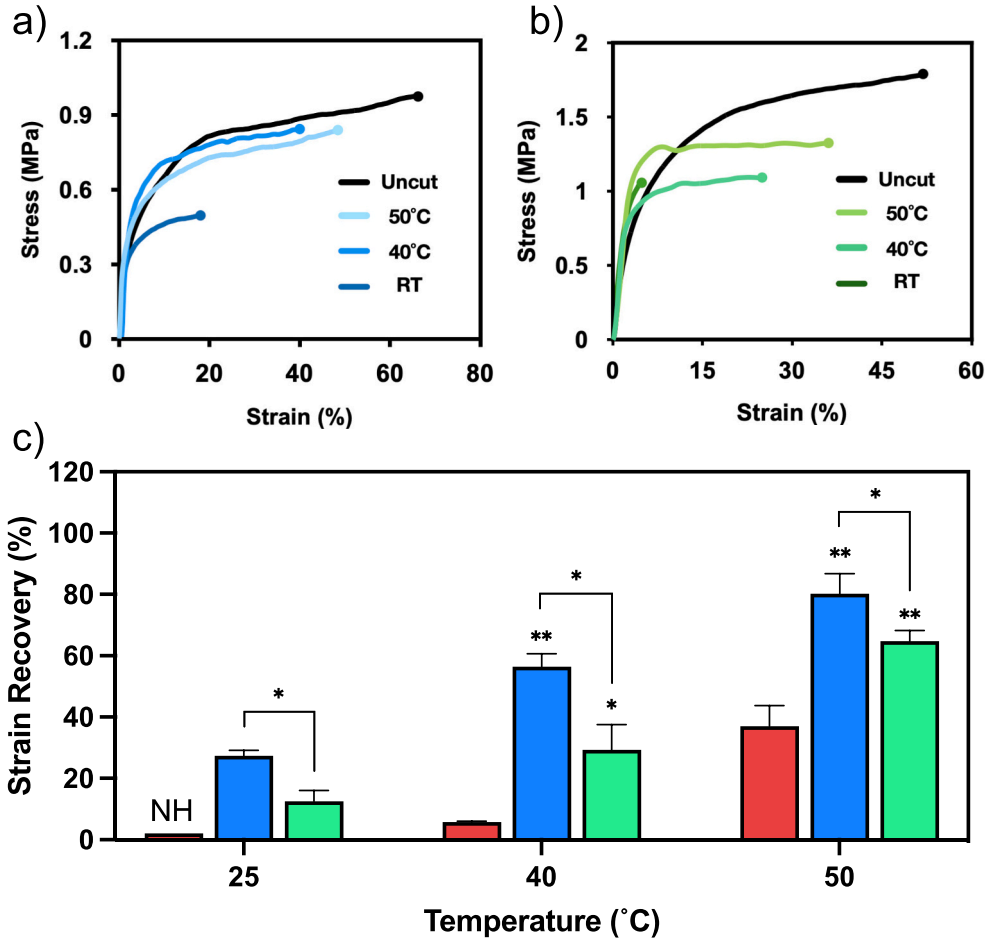


Fig. 6. Self-healing efficiency was evaluated via strain recovery tests of the uncut coatings compared with the cut coatings allowed to heal for 24 h over temperatures ranging from room temperature to 60 °C. a) An example stress strain curve for the UPy-2 coating. b) An example stress strain curve for the UPy-3 coating. c) The self-healing efficiency of the control (red), UPy-2 (blue) and UPy-3 (green) coatings for 25, 40 and 50 °C self-healing temperatures. NH indicates that no healing was observed. The data represents mean ± SD for $n = 3$ independent experiments. An unpaired *t*-test was used to analyze the statistical differences between the self-healing efficiency of each coating. * indicates $p \leq 0.05$, ** indicates $p \leq 0.01$. (For interpretation of the references to colour in this figure legend, the reader is referred to the web version of this article.)

recovery for all three samples is very strong, which implies that at very high temperatures, the heightened polymer dynamics of an MMA/BA/AA acrylic coating can spontaneously self-heal by means analogous to melting (the most basic self-healing mechanism). It is important to note that because all three coatings have a similar Young's modulus and Tg, self-healing is not occurring in the UPy functionalized coatings because they are inherently soft materials relative to the control. Rather, the self-complementary hydrogen bonding of the UPy unit itself is responsible for a significant fraction of self-healing performance. Interestingly, the MMA/BA/AA control coating begins to display self-healing activity >50 °C, likely due to the enhanced rheological properties of the polymers. However, the large difference between the self-healing efficiencies of the control and UPy-2 coatings even at this elevated temperature (from ~30 % and ~80 % respectively) emphasizes the self-healing power of the UPy hydrogen bonding design.

One of the principal benefits of intrinsic self-healing is the potential to repeatedly heal damage in the same area of a coating. This is an advantage that microcapsule-based extrinsic designs lack, given their single-use encapsulated healing agent. To test whether our UPy-2 and UPy-3 self-healing designs provided any repeatable self-healing, we subjected the coatings to self-healing cycles. A crack was introduced, and the coating was left to heal over 24 h at room temperature, after which the same crack was re-cut and reopened and allowed to heal again over the given conditions. This was repeated four times and the healing efficiency was recorded for each cycle (Fig. S23). The results are shown in Fig. 7a.

Fig. 7a displays the measured strain recovery (healing efficiency) of the UPy-2 and UPy-3 coatings over four healing cycles at room temperature. Both coatings have repeatable self-healing capability which seems to degrade with each cycle. The UPy-2 coating's self-healing efficiency is notable for cycles 1–3, decreasing from ~28 % to ~15 % and finally to ~8 %, however by cycle 4 the efficiency has dropped to insignificant levels. The UPy-3 coating, whose healing efficiency is already lower than the UPy-2 coating, displays repeatable self-healing only after 2 cycles, where the healing drops from ~12 % in cycle 1 to ~5 % in cycle 2. No self-healing efficiency was observed after cycle 3. Both coatings seem to lose their self-healing performance completely after 4 cycles. This is an interesting observation, given that intrinsic self-healing materials, unlike extrinsic materials, should theoretically be able to self-heal a given area of damage repeatedly, due to their inherent healing functionality.

To fully understand the ability of the UPy functionalized coatings to self-heal damage repeatedly, the experiment was repeated at 50 °C, the temperature at which self-healing efficiency for both coatings is at its highest (Figs. 7b, S24). Similar to the coatings at room temperature, self-healing efficiency decreases with each healing cycle. In the case of the UPy-2 coating, self-healing is observable for 2 cycles, before reducing to levels comparable to the control (shown by the red line in Fig. 7b). UPy-3, on the other hand, displays no repeatable self-healing whatsoever. Such a loss of repeatable healing efficiency as the number of healing cycles increases is frequently seen in other intrinsic self-healing designs, when repeatable self-healing is tested, and has been posited to be the result of damage to the coating during cycling [38,39]. One plausible reason for the observed reduction of repeatable self-healing efficiency in both the UPy-2 and UPy-3 coatings is that in the first healing cycle, both coatings are able to recover strain well into the plastic region of the material before the crack fails. This means that at the point of crack failure, the coatings have been permanently deformed into a 'crack open' position, so that when the experiment is repeated, self-healing efficiency is significantly reduced. A second explanation involves the fact that for each new healing/damage cycle, a greater number of unhealable bonds are broken. Given that the number of healable bonds in the same damage area does not change, the healing efficiency is thus minimized as more and more cycles are repeated. This mechanism of healing degradation, even in intrinsic self-healing systems, has been reported elsewhere [40,41]. Nevertheless, it is important to note that though self-healing efficiency decreases with each cycle, the UPy-2 coating does display repeatable self-healing both at room temperature and at 50 °C, which is a key advantage of an intrinsic self-healing material, and an important benefit for any self-healing organic coating.

4. Conclusion

Self-healing technology has been applied to various kinds of organic coatings including epoxy resins and polyurethane anti-corrosive coatings via the microencapsulation of healing agents, reversible covalent bond functionalization and supramolecular networks. However, self-healing studies based on waterborne acrylic latex coatings, which comprise the majority of trade paints, are noticeably lacking. We sought to design a self-healing acrylic latex which showed self-healing capability at room temperature and moderate conditions while maintaining its mechanical properties. We synthesized a library of acrylic monomers based on the strong hydrogen bonding unit UPy with varying amphiphilicity: UPy-1, UPy-2, UPy-3, and UPy-4. Of these four, UPy-2 and UPy-3, were able to undergo emulsion polymerization and form part of an MMA/BA acrylic latex. The resulting UPy-functionalized coatings displayed self-healing capability at room temperature, visually healing a crack and spontaneously recovering up to 28 % of their strain-at-break after 24 h. Self-healing efficiency was enhanced with elevated temperatures, and damage in the same spot was able to be healed repeatedly,

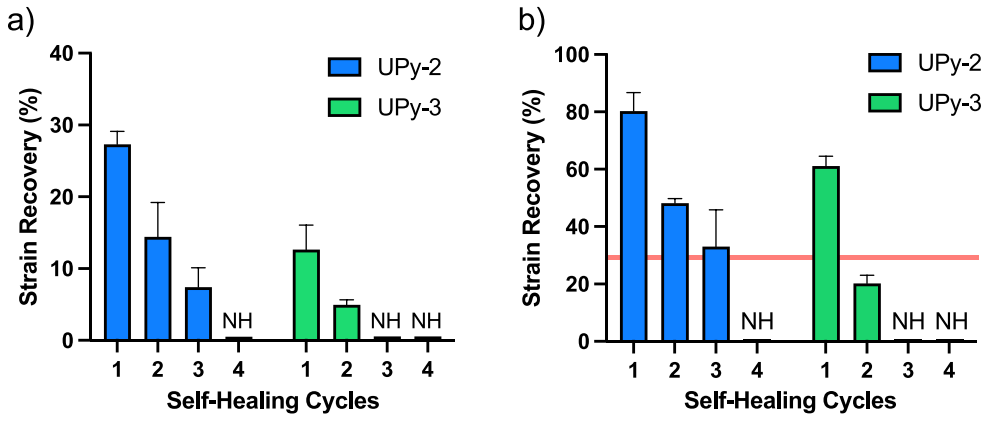


Fig. 7. Self-healing cycles for damage in the same area, which was healed and recut and healed again over four cycles. The cycles were conducted at RT and 50 °C with a healing time of 24 h. a) Healing cycles for the UPy-2 and UPy-3 coatings at RT. b) Healing cycles for the UPy-2 and UPy-3 coatings at 50 °C. NH refers to no observed self-healing relative to the control, and the red line in b) denotes the strain recovery of the control coating at 50 °C. (For interpretation of the references to colour in this figure legend, the reader is referred to the web version of this article.)

albeit with a noticeable decline in healing efficiency as the number of healing cycles increased. Comparing the self-healing efficiency of the UPy-2 and UPy-3 coatings also yielded important information regarding the mechanism of self-healing, and what factors influence self-healing efficiency in organic coatings. Furthermore, the UPy functionalized acrylic coatings maintained good mechanical strength, with Young's moduli ~200 MPa, one to two orders of magnitude above the hydrogels and elastomers commonly associated with intrinsic self-healing. Finally, our design did not alter the optical properties of the acrylic coatings, which remained transparent, nor was undesirable organic solvent introduced into the emulsion procedure. We believe this design is one of the first examples of latex acrylic self-healing at room temperature, without the often-accompanied loss of mechanical strength, and thus represents a significant step forward toward self-healing paint.

CRediT authorship contribution statement

Maximilian A. Beach: Data curation, Formal analysis, Investigation, Methodology, Writing – original draft, Writing – review & editing. **Tim W. Davey:** Conceptualization, Formal analysis, Investigation, Project administration, Resources, Supervision, Writing – review & editing. **Priya Subramanian:** Conceptualization, Resources, Writing – review & editing. **Georgina K. Such:** Conceptualization, Methodology, Project administration, Resources, Supervision, Writing – review & editing.

Declaration of competing interest

The authors declare that they have no known competing financial interests or personal relationships that could have appeared to influence the work reported in this paper.

Data availability

Data will be made available on request.

Acknowledgments

This work was supported by the Australian Research Council Discovery Project (DP180100844). Generous support from DuluxGroup Australia is gratefully acknowledged.

Appendix A. Supplementary data

Supplementary data to this article can be found online at https://doi.org/10.1016/j.porgcoat.2023.108189.

References

[1] Z.W. Wicks, F.N. Jones, S.P. Pappas, D.A. Wicks, Organic Coatings: Science and Technology, Wiley, 2007.
[2] S. García, H. Fischer, S. Van Der Zwaag, A critical appraisal of the potential of self healing polymeric coatings, Prog. Org. Coat. 72 (3) (2011) 211–221.
[3] S.R. White, N.R. Sottos, P.H. Geubelle, J.S. Moore, M.R. Kessler, S.R. Sriram, E. N. Brown, S. Viswanathan, Autonomic healing of polymer composites, Nature 409 (6822) (2001) 794–797.
[4] D.Y. Zhu, M.Z. Rong, M.Q. Zhang, Self-healing polymeric materials based on microencapsulated healing agents: from design to preparation, Prog. Polym. Sci. 49 (2015) 175–220.
[5] N. Wen, T. Song, Z. Ji, D. Jiang, Z. Wu, Y. Wang, Z. Guo, Recent advancements in self-healing materials: mechanicals, performances and features, React. Funct. Polym. 168 (2021) 105041.
[6] D.G. Bekas, K. Tsirka, D. Baltzis, A.S. Paipetis, Self-healing materials: a review of advances in materials, evaluation, characterization and monitoring techniques, Compos. B Eng. 87 (2016) 92–119.
[7] J.K. Lee, S.J. Hong, X. Liu, S.H. Yoon, Characterization of dicyclopentadiene and 5-ethylidene-2-norbornene as self-healing agents for polymer composite and its microcapsules, Macromol. Res. 12 (5) (2004) 478–483.
[8] T. Yin, M.Z. Rong, M.Q. Zhang, G.C. Yang, Self-healing epoxy composites—preparation and effect of the healant consisting of microencapsulated epoxy and latent curing agent, Compos. Sci. Technol. 67 (2) (2007) 201–212.
[9] H. Jin, C.L. Mangun, D.S. Stradley, J.S. Moore, N.R. Sottos, S.R. White, Self-healing thermoset using encapsulated epoxy-amine healing chemistry, Polymer 53 (2) (2012) 581–587.
[10] F. Ahangaran, M. Hayaty, A.H. Navarchian, Y. Pei, F. Picchioni, Development of self-healing epoxy composites via incorporation of microencapsulated epoxy and mercaptan in poly (methyl methacrylate) shell, Polym. Test. 73 (2019) 395–403.
[11] Y.-K. Song, C.-M. Chung, Repeatable self-healing of a microcapsule-type protective coating, Polym. Chem. 4 (18) (2013) 4940–4947.
[12] I.L. Hia, V. Vahedi, P. Pasbakhsh, Self-healing polymer composites: prospects, challenges, and applications, Polym. Rev. 56 (2) (2016) 225–261.
[13] N. Zhong, W. Post, Self-repair of structural and functional composites with intrinsically self-healing polymer matrices: a review, Compos. A: Appl. Sci. Manuf. 69 (2015) 226–239.
[14] S. Sung, S.Y. Kim, T.H. Lee, G. Favaro, Y.I. Park, S.-H. Lee, J.B. Ahn, S.M. Noh, J. C. Kim, Thermally reversible polymer networks for scratch resistance and scratch healing in automotive clear coats, Prog. Org. Coat. 127 (2019) 37–44.
[15] M. Liu, J. Zhong, Z. Li, J. Rong, K. Yang, J. Zhou, L. Shen, F. Gao, X. Huang, H. He, A high stiffness and self-healable polyurethane based on disulfide bonds and hydrogen bonding, Eur. Polym. J. 109475 (2020).
[16] F. Zhang, P. Ju, M. Pan, D. Zhang, Y. Huang, G. Li, X. Li, Self-healing mechanisms in smart protective coatings: a review, Corros. Sci. 144 (2018) 74–88.
[17] M. Cheng, Q. Fu, B. Tan, Y. Ma, L. Fang, C. Lu, Z. Xu, Build a bridge from polymeric structure design to engineering application of self-healing coatings: a review, Prog. Org. Coat. 167 (2022) 106790.
[18] Y. Yang, M.W. Urban, Self-healing of polymers via supramolecular chemistry, Adv. Mater. Interfaces 5 (17) (2018) 1800384.
[19] G. Thangavel, M.W.M. Tan, P.S. Lee, Advances in self-healing supramolecular soft materials and nanocomposites, Nano Converg. 6 (1) (2019) 29.
[20] R. Hoogenboom, Hard autonomous self-healing supramolecular materials—a contradiction in terms? Angew. Chem. Int. Ed. 51 (48) (2012) 11942–11944.
[21] Y. Chen, A.M. Kushner, G.A. Williams, Z. Guan, Multiphase design of autonomic self-healing thermoplastic elastomers, Nat. Chem. 4 (6) (2012) 467.
[22] Y. Chen, Z. Guan, Multivalent hydrogen bonding block copolymers self-assemble into strong and tough self-healing materials, Chem. Commun. 50 (74) (2014) 10868–10870.
[23] J. Hentschel, A.M. Kushner, J. Ziller, Z. Guan, Self-healing supramolecular block copolymers, Angew. Chem. Int. Ed. Engl. 51 (42) (2012) 10561–10565.
[24] F.H. Beijer, R.P. Sijbesma, H. Kooijman, A.L. Spek, E.W. Meijer, Strong dimerization of ureidopyrimidones via quadruple hydrogen bonding, J. Am. Chem. Soc. 120 (27) (1998) 6761–6769.
[25] T. Liu, H. Zhao, D. Zhang, Y. Lou, L. Huang, L. Ma, X. Hao, L. Dong, F. Rosei, W. M. Lau, Ultrafast and high-efficient self-healing epoxy coatings with active multiple hydrogen bonds for corrosion protection, Corros. Sci. 187 (2021) 109485.
[26] J. Hu, R.B. Mo, X. Jiang, X.X. Sheng, X.Y. Zhang, Towards mechanical robust yet self-healing polyurethane elastomers via combination of dynamic main chain and dangling quadruple, Polymer 183 (2019).
[27] Cui, X. Y.; Zhang, C.; Camilo, R. P.; Zhang, H.; Cobaj, A.; Soucek, M. D.; Zacharia, N. S., Self-healing latex containing polyelectrolyte multilayers. Macromol. Mater. Eng. 2018, 303 (8).
[28] T. Qiu, X.J. Wang, X.Y. Lin, Z.Q. Zhu, X.Y. Li, L.H. Guo, Emulsion polymerization to synthesize self-healing films toward healing on fractures: a feasible strategy, J. Polym. Sci. A Polym. Chem. 54 (19) (2016) 3071–3078.
[29] Y. Chen, S.T. Jones, I. Hancox, R. Beanland, E.J. Tunnah, S.A.F. Bon, Multiple hydrogen-bond array reinforced cellular polymer films from colloidal crystalline assemblies of soft latex particles, ACS Macro Lett. 1 (5) (2012) 603–608.
[30] J. Zhang, S. Qi, C. Zhang, Z. Fan, Q. Ding, S. Mao, Z. Dong, Controlling keto–enol tautomerism of ureidopyrimidinone to generate a single-quadruple AADD-DDAA dimeric array, Org. Lett. 22 (18) (2020) 7305–7309.
[31] W.P.J. Appel, G. Portale, E. Wisse, P.Y.W. Dankers, E.W. Meijer, Aggregation of ureido-pyrimidinone supramolecular thermoplastic elastomers into nanofibers: a kinetic analysis, Macromolecules 44 (17) (2011) 6776–6784.
[32] X. Liu, T. Gallavardin, F. Burel, D. Vuluga, Influence of quadruple hydrogen bonding on polyvinyl butyral resin properties, Polym. Degrad. Stab. 208 (2023) 110243.
[33] A. Faghihnejad, K.E. Feldman, J. Yu, M.V. Tirrell, J.N. Israelachvili, C.J. Hawker, E. J. Kramer, H. Zeng, Adhesion and surface interactions of a self-healing polymer with multiple hydrogen-bonding groups, Adv. Funct. Mater. 24 (16) (2014) 2322–2333.
[34] S. Mirabedini, I. Dutil, L. Gauquelin, N. Yan, R.R. Farnood, Preparation of self-healing acrylic latex coatings using novel oil-filled ethyl cellulose microcapsules, Prog. Org. Coat. 85 (2015) 168–177.
[35] S. Chen, N. Mahmood, M. Beiner, W.H. Binder, Self-healing materials from V- and H-shaped supramolecular architectures, Angew. Chem. Int. Ed. Engl. 54 (35) (2015) 10188–10192.
[36] L. Zhang, D. Wang, L. Xu, X. Zhang, A. Zhang, Y. Xu, A highly stretchable, transparent, notch-insensitive self-healing elastomer for coating, J. Mater. Chem. C 8 (6) (2020) 2043–2053.
[37] A.M. Kushner, J.D. Vossler, G.A. Williams, Z. Guan, A biomimetic modular polymer with tough and adaptive properties, J. Am. Chem. Soc. 131 (25) (2009) 8766–8768.
[38] M.Q. Zhang, M.Z. Rong, Application of alkoxyamine in self-healing of epoxy, J. Mater. Chem. A 2 (18) (2014) 6558–6566.

[39] J. Ling, M.Z. Rong, M.Q. Zhang, Coumarin imparts repeated photochemical remendability to polyurethane, J. Mater. Chem. 21 (45) (2011) 18373–18380.
[40] Y. Heo, M.H. Malakooti, H.A. Sodano, Self-healing polymers and composites for extreme environments, J. Mater. Chem. A 4 (44) (2016) 17403–17411.
[41] B. Guo, X. Ji, X. Chen, G. Li, Y. Lu, J. Bai, A highly stretchable and intrinsically self-healing strain sensor produced by 3D printing, Virtual Phys. Prototyp. 15 (sup1) (2020) 520–531.